Truss optimization applying finite element limit analysis including global and local stability

Poulsen, Peter Noe; Olesen, John Forbes; Baandrup, Mads Jacob

Published in:
Structural and Multidisciplinary Optimization

Link to article, DOI:
10.1007/s00158-019-02468-4

Publication date:
2020

Document Version
Peer reviewed version

Structural and Multidisciplinary Optimization manuscript No.
(will be inserted by the editor)

Truss optimization applying finite element limit analysis including global and local stability

Peter Noe Poulsen · John Forbes Olesen · Mads Baandrup

Received: date / Accepted: date

Abstract For practical applications of optimized truss structures, it is essential to include global and local stability in order to obtain stable and realistic structures. The challenge of including both global and local stability has previously been approached in many ways. However, these proposals often lead to ill-conditioned optimization problems, with convergence issues due to the concavity of the problem. In this paper, a new method for handling both global and local stability in truss optimization is presented. The proposed method is based on the Finite Element Limit Analysis method. Initially, the global stability problem is solved by a convex semidefinite constraint, and subsequently, the concave local stability problem is included through an iterative process, where the local stability constraints are linearized and solved by a convex sub-problem. This step-wise approach diminishes convergence issues due to the concavity of the problem. The proposed method is demonstrated through three different applications showing significant effects of including global and local stability in the optimized designs, while at the same time demonstrating the validity and potential of the proposed method.

Keywords Truss topology optimization · Global stability · Convex problem · Limit analysis

Peter Noe Poulsen · John Forbes Olesen
Department of Civil Engineering, Technical University of Denmark, Brovej B.118, 2800 Kgs. Lyngby, Denmark
E-mail: pnp@byg.dtu.dk

Mads Baandrup
Department of Civil Engineering, Technical University of Denmark, Brovej B.118, 2800 Kgs. Lyngby, Denmark
Department of Major Bridges International, COWI A/S, Parallelvej 2, 2800 Kgs. Lyngby, Denmark
E-mail: mjba@byg.dtu.dk

Acknowledgements The presented work is part of an industrial ph.d. project with the title "Innovative design of steel bridge girders in cable supported bridges" and is carried out in cooperation with COWI A/S, DTU Civil Engineering and DTU Mechanical Engineering. The project is supported financially by the COWI Foundation grant C-131.02 and Innovation Fund Denmark grant 5189-00112B.

1 Introduction

Truss structures are by nature, simple and transparent structures, which efficiently carry the applied loads to the supports. For these reasons, trusses have been applied for centuries in all sorts of structures. Because of this efficiency, and their apparent simplicity, trusses have been subject to numerical optimization for decades. Truss topology optimization often leads to lightweight structures prone to instabilities which must be dealt with in order to obtain realistic structures.

The first numerical investigations of optimal truss structures were performed more than fifty years ago in Dorn et al. (1964) introducing a ground structure, with the cross sectional areas as continuous design variables. The problem was formulated as a Linear Programming (LP) problem including the equilibrium equations and minimizing the weight, under the assumption that the material consumption was linearly related to the numerical size of the normal forces. This assumption was based on utilizing the material to its yield stress. It was shown that the result of this optimization under plastic conditions was also an optimal structure under elastic conditions when considering a single load configuration.

A few years later, a numerical method for modeling the ultimate load of structures assuming a rigid-plastic material behavior was formulated, Anderheggen and Knöpfel (1972). The Finite Element Limit Anal-

ysis (FELA), by both the lower bound approach and the upper bound approach, was introduced according to the classic plasticity theory.

Pedersen (1972) included local stability in an early formulation for obtaining the elastic optimal layout of trusses. The formulation included position of the joints and restriction on displacements and was solved using LP in an iterative procedure.

In practical applications of optimized trusses, it is crucial to obtain an overall stable structure. However, several challenges arise when implementing this requirement, as discussed in Zhou (1996); Rozvany (1996), and many different approaches to overcome them have been proposed. One suggestion to secure an overall stable structure (as supporting bars may approach zero) was the introduction of so-called chains to account for the change in effective buckling lengths Achtziger (1999a,b). A more direct way to handle the global stability phenomenon is by including the interaction between the individual members. In Ben-Tal et al. (2000); Kočvara (2002) the global stability was handled, setting up the linear buckling problem. Due to an elastic distribution of forces, the formulation resulted in a non-convex semidefinite programming problem. Other ways of handling the global stability have been investigated, see e.g. Descamps and Filomeno Coelho (2014) where it was handled by a perturbation of the nodal coordinates, and Guo et al. (2005); Torii et al. (2015); Changizi and Jalalpour (2017) where the constraint was based on predetermined overall buckling modes for the structure, found by eigenvalue analysis. The problem has also been treated applying beam elements in Torii et al. (2015); Changizi and Jalalpour (2017); Madah and Amir (2017) eliminating the local buckling at the cost of a larger global stability problem.

Finding the optimal solution in a non-convex problem is not a simple task, and the search may involve many different attempts and much computational effort. Related to this search for the optimal solution Evgrafov (2004) describes the so-called global stability singularity problem where the optimal solution is not connected to the interior of the solution domain. This shows the difficulties related to finding optimal solutions applying an elastic distribution of forces. It has been stated in Tugilimana et al. (2018) that the problem was alleviated by stating a disaggregated form of the equilibrium as a two-step elastic relation. Very recently Weldeyesus et al. (2019) presented a so-called relaxed formulation of the elastic optimal truss layout, including global stability but disregarding the kinematic compatibility and local stability. This, in fact, corresponds to a rigid plastic force distribution and results in a convex semidefinite problem.

It may seem contradictory to apply both a rigid plastic force distribution and a linear buckling problem assuming an elastic behaviour but for a single load configuration it was previously shown that the result of a plastic optimization is also an optimal structure under elastic conditions and therefore the behaviour of the structure will be elastic until the critical load level where it yields and buckles simultaneously. When optimizing the structure considering multiple load cases bars may yield or buckle before the maximum load. The characteristic load-displacement behaviour of bars that buckle is similar to bars that yield and in this respect the model is still valid. The overall behaviour of truss structures that has been optimized for multiple load cases has been investigated, see Mikkelsen (2018), and it was shown by a non-linear geometric analysis that the structure was able to carry load after the first buckling and reach the intended load level.

Since the introduction of plastic optimization, by application of FELA, the method has been developed to handle various kinds of elements, such as beams and slabs Damkilde and Høyer (1993); Krenk (1994). Particularly, in recent years the method has been applied in the analysis of soil mechanics, Krabbenhoft et al. (2005); Akhlaghi (2006); Lyamin (2009), and in the analysis of reinforced concrete disks, slabs and joints, Poulsen and Damkilde (2000); Herfelt et al. (2016, 2017); Herfelt (2017); Herfelt et al. (2018). Recently, the method was applied in the optimization of continuum structures Fin et al. (2018); Herfelt et al. (2019), but so far it has not been applied in truss optimization including global and local stability.

In this paper, a method based on FELA is proposed to solve the problem of truss optimization including global and local stability.

Firstly, the truss optimization problem is solved considering only global stability. The global stability is formulated through the linear buckling problem introducing a semidefinite constraint, preserving the convexity of the problem. Secondly, the local buckling constraint is introduced through the critical Euler buckling load, making the overall problem non-convex. However, the problem can be solved step-wise by a linearization of the local buckling constraint. Hence, the overall concave problem, including global and local stability, is solved in an iterative process with convex sub-problems.

To demonstrate the validity of the proposed method, three plane cases are studied; a simple two-bar structure, a tip-loaded cantilever beam, and a vertically load column. The study of the stability for a simple two-bar structure allows for comparison against an analytical solution. The cantilever beam study exhibits the effect of increasing mesh density and convergence properties,

as well as demonstrates the capability of handling multiple load cases. Additionally, the effects on the design of first adding the global stability constraint and subsequently, the local buckling constraint are shown. The column study gives insight into the importance of using realistic material parameters when including stability in truss optimization. Finally, the effects on the truss layout from increasing column slenderness is studied.

2 Truss layout optimization

The structures studied in this paper are trusses defined by N nodal points in a 2-dimensional space $d = 2$. The number of supports is denoted N_s and the number of equilibrium equations is $N_d = d \cdot N - N_s$. The number of elements in the structure is given by N_e and the topology design variable is given as the element areas a_e collected in $\mathbf{A}^{[N_e \times 1]}$. Similarly, the element lengths are collected in $\mathbf{L}^{[N_e \times 1]}$. The total truss volume is thus given by

$$V = \sum_{e=1}^{N_e} a_e \ell_e = \mathbf{A}^\top \mathbf{L} \tag{1}$$

2.1 Finite element limit analysis

The finite element limit analysis is a method assuming perfect plastic materials. The material models are simplified assuming a rigid behaviour prior to plasticity. The method is based on the finite element method, as all variables, equations, and inequalities are either node or element based. However, the load-deflection path is not determined, as no deformations occur before yielding. Unlimited deformation capacity is assumed, only the collapse mode is found, and small displacements are assumed. The yield criterion is a convex surface in the stress space. The mathematical problem of FELA is formulated as a convex optimization problem which can be solved very efficiently by state-of-the-art solvers. The reader is referred to Anderheggen and Knöpfel (1972); Damkilde and Høyer (1993); Poulsen and Damkilde (2000); Krabbenhøft et al. (2008) for an in-depth introduction to the method.

The pure volume optimization formulation contains two parts. The first part, the equilibrium equations, ensures equilibrium in all nodal forces in the structure, hence ensures a statically admissible solution. The second part, the yield condition, ensures all element stresses to be within the yield criterion.

The bar element with a constant normal force, $N_e = \beta_e$, together with the element nodal forces, is shown in Fig. 1. The element nodal forces, with respect to the local element axes, can be written as

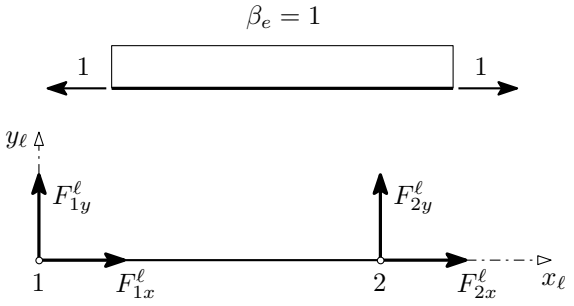

Fig. 1 Stress interpolation and nodal forces of an equilibrium bar element

$$\begin{bmatrix} F^\ell_{1x} \\ F^\ell_{1y} \\ F^\ell_{2x} \\ F^\ell_{2y} \end{bmatrix} = \begin{bmatrix} -1 \\ 0 \\ 1 \\ 0 \end{bmatrix} \beta_e \quad \Leftrightarrow: \quad \mathbf{q}_e = \mathbf{h}^\ell_e \boldsymbol{\beta}_e \tag{2}$$

where $\mathbf{q}_e$ is the element nodal force vector, $\mathbf{h}^\ell_e$ is the element equilibrium matrix, and $\boldsymbol{\beta}_e$ is the element stress vector.

The global equilibrium matrix $\mathbf{H}^{[N_d \times N_e]}$ is assembled in the standard way

$$\mathbf{H} = \sum_{e=1}^{N_e} \mathbf{H}_e \quad \text{with} \quad \mathbf{H}_e(\mathbf{d}_e, \mathbf{d}_{\beta_e}) = \mathbf{T}^\top_e \mathbf{h}_e \tag{3}$$

where $\mathbf{d}^{[2d]}_e$ is an index vector mapping from the local to the global equation numbers, $\mathbf{d}^{[2d]}_{\beta_e}$ is an index vector mapping from the local to the global stress parameters, and $\mathbf{T}^{[2d \times 2d]}_e$ is the transformation matrix from local to global coordinates. The equilibrium equations can now be written as

$$\mathbf{H}\boldsymbol{\beta} = \mathbf{R} \tag{4}$$

where $\boldsymbol{\beta}^{[N_d \times 1]}$ is a vector collecting all β_e and $\mathbf{R}^{[N_d \times 1]}$ is a vector containing external nodal loads.

The yield condition for a bar element and thereby the restrictions on the normal force can be given by the tension and compression normal capacities, $N^+_{y,e}$ and $N^-_{y,e}$, and expressed by the yield stress and the cross sectional area, f_y and a_e

$$\begin{bmatrix} 1 \\ -1 \end{bmatrix} \beta_e \le \begin{bmatrix} N^+_{y,e} \\ N^-_{y,e} \end{bmatrix} = \begin{bmatrix} f_y \\ f_y \end{bmatrix} a_e \quad \Leftrightarrow: \quad \mathbf{c}_e \boldsymbol{\beta}_e \le \mathbf{c}_{m,e} \mathbf{a}_e \tag{5}$$

where $\mathbf{c}_e$ and $\mathbf{c}_{m,e}$ are restriction matrices for the element and $\mathbf{a}_e$ contains the cross sectional area for the element. The restriction matrices can be assembled similarly to $\mathbf{H}$ by use of $\mathbf{C}_e(\mathbf{d}_{c_e}, \mathbf{d}_{\beta_e}) = \mathbf{c}_e$ and $\mathbf{C}_{m,e}(\mathbf{d}_{c_e}) =$

$\mathbf{c}_{m,e}$, where $\mathbf{d}_{c_e}$ is an index vector mapping from the local to the global restriction numbers. In matrix notation the yield conditions for the system can be given as

$$\mathbf{C}\boldsymbol{\beta} - \mathbf{C}_m\mathbf{A} \leq \mathbf{0} \tag{6}$$

where $\mathbf{C}^{[2N_e \times N_e]}$ transforms the bar forces and $\mathbf{C}_m^{[2N_e \times N_e]}$ contains the yield stresses.

Thus, the linear optimization problem (LP) for pure volume optimization is given as

$$\min_{\boldsymbol{\beta},\,\mathbf{A}} \quad \mathbf{A}^\top\mathbf{L} \tag{7a}$$

$$\text{s.t.} \quad \mathbf{H}\boldsymbol{\beta} = \mathbf{R} \tag{7b}$$

$$\mathbf{C}\boldsymbol{\beta} - \mathbf{C}_m\mathbf{A} \leq \mathbf{0} \tag{7c}$$

The problem with linear equality and inequality constraints is convex, and very efficient convex solvers may be utilized.

For N_k multiple load cases the equilibrium equations must be set up for each load case with separate stress parameters. This can be handled by replacing the matrices and vectors in the optimization problem with a collection of sub-matrices and sub-vectors as shown for the equilibrium equations

$$\mathbf{H} = \begin{bmatrix} \mathbf{H}_1 & & \\ & \ddots & \\ & & \mathbf{H}_k \end{bmatrix}, \quad \boldsymbol{\beta} = \begin{bmatrix} \boldsymbol{\beta}_1 \\ \vdots \\ \boldsymbol{\beta}_k \end{bmatrix}, \quad \mathbf{R} = \begin{bmatrix} \mathbf{R}_1 \\ \vdots \\ \mathbf{R}_k \end{bmatrix} \tag{8}$$

where index k indicates the part corresponding to load case k. Similarly for the yield restrictions

$$\mathbf{C} = \begin{bmatrix} \mathbf{C}_1 & & \\ & \ddots & \\ & & \mathbf{C}_k \end{bmatrix}, \quad \mathbf{C}_m = \begin{bmatrix} \mathbf{C}_{m,1} \\ \vdots \\ \mathbf{C}_{m,k} \end{bmatrix} \tag{9}$$

The problem now consists of $n = N_e \cdot (N_k + 1)$ optimization variables and $m = m_H + m_C = N_d \cdot N_k + 2N_e \cdot N_k$ constraint functions.

In the formulation of finite element limit analysis, multiple load cases are in general handled by an expansion of the system of equations, as mentioned in the above. The number of design variables and constraints thus increases (almost) linearly with the number of load cases. The size of the constraint matrices increases quadratically, however, as all matrices are defined sparse, the actual problem size increases linearly.

2.2 Global stability as semidefinite constraint

To constrain the optimized structures from global stability problems, a semidefinite constraint is introduced on the sum of the elastic and geometric stiffness matrices. In a standard linear elastic finite element analysis, the elastic matrix is introduced to relate displacements and forces in the structure, and the geometric matrix is introduced to handle large deformations. However, in the present formulation, the stiffness matrices are solely introduced to handle the global stability phenomenon.

The local elastic stiffness matrix is given as

$$\mathbf{k}_e = a_e \int_0^{\ell_e} \tfrac{E}{\ell_e}\mathbf{B}^\top\mathbf{B}dx = \tfrac{E\,a_e}{\ell_e}\begin{bmatrix} 1 & 0 & -1 & 0 \\ 0 & 0 & 0 & 0 \\ -1 & 0 & 1 & 0 \\ 0 & 0 & 0 & 0 \end{bmatrix} = a_e\mathbf{k}_{0,e} \tag{10}$$

where $\mathbf{B}^{[1\times 2d]}$ is the strain interpolation matrix and E the modulus of elasticity. For the optimization problems the stiffness matrix is defined as $\mathbf{k}_{0,e}$ leaving out the area a_e. The global elastic stiffness matrix $\mathbf{K}(\mathbf{A})^{[N_d \times N_d]}$, defined as a function of the design variables $\mathbf{A}$, is assembled in the usual way

$$\begin{aligned} \mathbf{K}(\mathbf{A}) &= \sum_{e=1}^{N_e} \mathbf{K}_e(\mathbf{A}) \\ \text{with } \mathbf{K}_e(\mathbf{A})(\mathbf{d}_e, \mathbf{d}_e) &= a_e\mathbf{T}_e^\top\mathbf{k}_{0,e}\mathbf{T}_e \end{aligned} \tag{11}$$

where $\mathbf{d}_e^{[2d]}$ is an index vector mapping from the local to the global system and $\mathbf{T}_e^{[2d\times 2d]}$ is the transformation matrix from local to global coordinates.

The local geometric stiffness matrix is given as

$$\mathbf{k}_{G,e} = \beta_e \int_0^{\ell_e} \mathbf{G}^\top\mathbf{G}dx = \tfrac{\beta_e}{\ell_e}\begin{bmatrix} 0 & 0 & 0 & 0 \\ 0 & 1 & 0 & -1 \\ 0 & 0 & 0 & 0 \\ 0 & -1 & 0 & 1 \end{bmatrix} = \beta_e\mathbf{k}_{G,0,e} \tag{12}$$

where $\mathbf{G}^{[2d\times 2d]}$ is the gradient shape function interpolation matrix. For the optimization problems the stiffness matrix is defined as $\mathbf{k}_{G,0,e}$ without the variable β_e. The global stiffness matrix $\mathbf{K}_G(\boldsymbol{\beta})^{[N_d \times N_d]}$, defined as a function of the design variables $\boldsymbol{\beta}$, is assembled in the usual way

$$\begin{aligned} \mathbf{K}_G(\boldsymbol{\beta}) &= \sum_{e=1}^{\text{nel}} \mathbf{K}_{G,e}(\boldsymbol{\beta}) \\ \text{with } \mathbf{K}_{G,e}(\boldsymbol{\beta})(\mathbf{d}_e, \mathbf{d}_e) &= \beta_e\mathbf{T}_e^\top\mathbf{k}_{G,0,e}\mathbf{T}_e \end{aligned} \tag{13}$$

The linear eigenvalue problem defining the global stability limit, see e.g. Cook et al. (1989), is given as

$$(\mathbf{K} + \lambda\mathbf{K}_G)\mathbf{v} = \mathbf{0} \tag{14}$$

with eigenvalue λ and corresponding eigenvector $\mathbf{v}$. Here, a priori, the load parameter/eigenvalue is $\lambda = 1$, and the buckling condition is governed by the design variables $\boldsymbol{\beta}$ and $\mathbf{A}$. A sufficient condition for this eigenvalue problem to be fulfilled, and thereby for global stability to be ensured, is to demand the summed stiffness matrix $\mathbf{K}_S$ to be positive definite

$$\mathbf{K}_S = \mathbf{K}_G(\boldsymbol{\beta}) + \mathbf{K}(\mathbf{A}) \succeq 0 \tag{15}$$

Adding the positive semidefinite constraint (15) to the LP (7) for N_k load cases, the semidefinite optimization problem (SDP) with linear objective function is given as

$$\min_{\boldsymbol{\beta},\,\mathbf{A}} \quad \mathbf{A}^\top \mathbf{L} \tag{16a}$$

$$\text{s.t.} \quad \mathbf{H}\boldsymbol{\beta} = \mathbf{R} \tag{16b}$$

$$\mathbf{C}\boldsymbol{\beta} - \mathbf{C}_m\mathbf{A} \leq \mathbf{0} \tag{16c}$$

$$\mathbf{K}_G(\boldsymbol{\beta}_k) + \mathbf{K}(\mathbf{A}) \succeq 0 \;\forall\, k = 1, \ldots, N_k \tag{16d}$$

The above optimization problem is equivalent to the formulation of the dual problem in the Mosek optimization software MOSEK (2018a), which is used as the solver. The constraint (16d) is thus, for a single load case, handled as a linear matrix inequality (LMI) in the form

$$\mathbf{K}_S = \mathbf{K}_G(\boldsymbol{\beta}_k) + \mathbf{K}(\mathbf{A}) = \mathbf{S}, \quad \mathbf{S} \succeq 0 \tag{17}$$

where $\mathbf{K}_S$ is converted to a set of linear equality constraints using an implicit semidefinite slack variable $\mathbf{S}$. The semidefinite requirement is thus moved from being explicit on $\mathbf{K}_S$ to being implicit on $\mathbf{S}$. The extra constraints add $m_K = N_k \times N_d \cdot (N_d + 1)/2$ linear equality constraint functions to the problem, equivalent to the number of elements in the lower triangular part of $\mathbf{K}_S$ times the number of load cases. The slack variables $\mathbf{S}$ adds N_k semidefinite constraints.

2.3 Local buckling constraint

It is essential to include the local stability of individual members in the optimization when striving towards realistic truss structures. For truss members, only subject to normal forces, local stability can be ensured by imposing that the internal compression force is limited by the critical buckling load. By introducing the critical Euler buckling load for a simply supported member, the local buckling constraint for element e is given as

$$-\beta_e \leq P_{cr,e} = \frac{\pi^2 \cdot EI_e}{\ell_e^2} \tag{18}$$

where I_e is the second moment of area. As tension members have positive normal forces $\beta_e \geq 0$, the constraint is only active for compression members where $\beta_e \leq 0$.

Due to the non-linear second moment of area, the constraint is not linear in regard of the design variable a_e. To implement the constraint into the optimization problem a first step is thus to reformulate it into a quadratic function of the cross section area a. For a solid rod, with $I_{\text{rod}} = \frac{a^2}{4\pi}$, the critical Euler load is simplified to

$$P_{cr,\text{rod}} = \frac{\pi^2 \cdot E}{l^2}\frac{a^2}{4\pi} = \frac{\pi \cdot Ea^2}{4l^2} = \alpha \cdot a^2 \tag{19}$$

where a constant α-factor is introduced, which for the rod is $\alpha_{\text{rod}} = \frac{\pi \cdot E}{4l^2}$. Similarly, this can be done for thin tubes if the ratio between the tube diameter D and shell thickness t is fixed by a constant γ given as $\frac{D}{t} = \gamma$. Then, the tube area can be defined as $a = \pi\gamma t^2$ and the second moment of area as $I_{\text{tube}} = \frac{\gamma}{8\pi}a^2$. The α-factor in (19) can thus for a thin tube be replaced by $\alpha_{\text{tube}} = \frac{\gamma \cdot \pi \cdot E}{8l^2}$. In the following, this expression for α is used together with the Eurocode 3 expression for γ, given for thin tubes with class 1 cross sections (fully plastic) as

$$\gamma = 50 \cdot \frac{235\text{MPa}}{f_y} \tag{20}$$

where the yield stress f_y is given in MPa. Thin tubes are thus assumed as the truss members. However, the expression for α can be modified to many types of cross sections using reasonable assumptions, see e.g. Changizi and Jalalpour (2017).

The simplified local buckling constraint can thus in general be defined as

$$-\beta_e \leq P_{cr,e} \simeq \alpha_e a_e^2 \tag{21}$$

However, the above inequality is concave, hence it cannot immediately be integrated in the formulation of the convex optimization problem.

2.3.1 Linearization of Euler stability

To include the concave inequality constraint (21) in the convex optimization formulation, the constraint is linearized. Since this is a significant simplification, the linearized equations are updated in an iterative process until convergence. The procedure of linearization is established in the following, whereas the iterative implementation is presented in Sec. 2.3.2. The idea of handling the Euler stability criterion by an iterative process was also discussed in Parkes (1975) and He and Gilbert (2015).

The general feasible solution domain for element e is shown in Fig. 2. For tension forces ($\beta_e \geq 0$) the domain is constrained by the yield criterion $f_y a_e$. For compression forces ($\beta_e \leq 0$) it is constrained by the quadratic constraint (21) for $0 \leq a_e \leq \frac{f_y}{\alpha_e}$ and by the yield criterion $-f_y a_e$ for $\frac{f_y}{\alpha_e} \leq a_e$.

The quadratic expression for P_{cr} in (21) is linearized in two different ways, tangent and secant, dependent

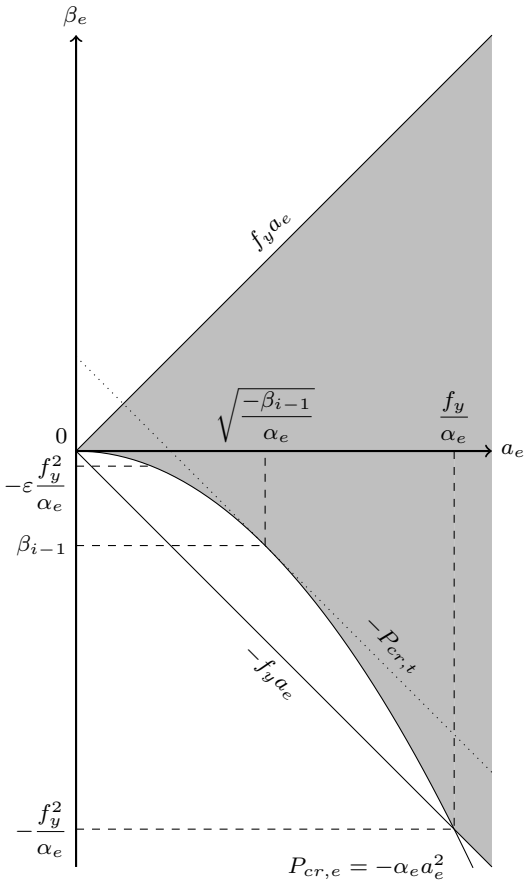

Fig. 2 Feasible solution domain for element e shown in gray. The stress-limit functions are given as functions of a_e. Tangent linearization of P_{cr} is shown as a dotted line, with indication of intersection with $P_{cr,e}$

on the member force β_e. The tangent is used as linearization when $\beta_e < -\varepsilon\frac{f_y^2}{\alpha_e}$, where ε is a small number ($\varepsilon = 10^{-3}$), hence for most compression members. The tangent $P_{cr,t}$ is shown in Fig. 2 and given as

$$P_{cr,t} \;=\; 2\alpha a_{i-1} a_i \;-\; \alpha a_{i-1}^2 \tag{22}$$

where i refers to the current iteration, and $i-1$ refers to the previous iteration in the iterative process. The linearization is thus based upon the solution to a previous solved optimization problem, which is discussed more in detail in Sec. 2.3.2. To ensure a stable algorithm a_{i-1} is not directly used from the previous solution, but calculated based on the truss force from the previous optimization problem as

$$a_{i-1} \;=\; \sqrt{\frac{-\beta_{i-1}}{\alpha}} \tag{23}$$

The tangent is used for most compression members due to it being a conservative simplification. However, the tangent also explicitly imposes a minimum area on the

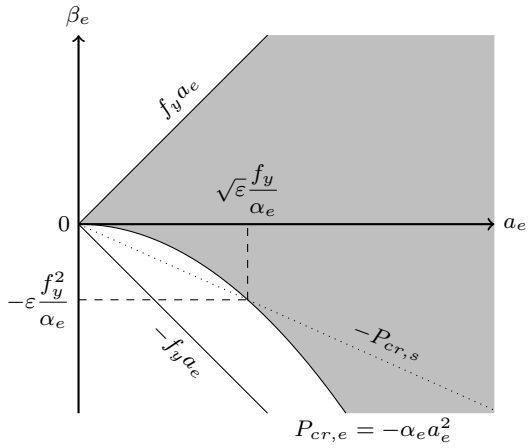

Fig. 3 Partial enlargement of Fig. 2. Secant linearization of P_{cr} is shown as a dotted line, with indication of intersection with $P_{cr,e}$

member, given at the intersection with the abscissa (see Fig. 2). To handle this misbehaviour a secant is used for linearization when $\beta_e \geq -\varepsilon\frac{f_y^2}{\alpha_e}$, hence for compression members with very small compression forces and tension members in general. The secant $P_{cr,s}$ is shown in Fig. 3 and given as

$$P_{cr,s} \;=\; \alpha a_{i-1} a_i \;=\; \sqrt{\varepsilon} f_y a_i \tag{24}$$

where the term a_{i-1} has been fixed as

$$a_{i-1} \;=\; \sqrt{\varepsilon}\frac{f_y}{\alpha_e} \tag{25}$$

By using the (non-conservative) secant, member areas are allowed to vanish during the optimization.

From the tangent (22) and secant (24) linearizations the Euler stability criterion can be formulated generally as a linear inequality constraint in the form

$$-\beta_e \;-\; p_e a_e \leq q_e \tag{26}$$

where p_e is the slope of the linearization and q_e the intersection with the ordinate in Fig. 2 and 3. The constraint (26) in matrix form is given as

$$-\mathbf{I}\boldsymbol{\beta} \;-\; \mathbf{P}\mathbf{A} \leq \mathbf{q} \tag{27}$$

where $\mathbf{I}^{[N_e \cdot N_k \times N_e \cdot N_k]}$ is the identity matrix, $\mathbf{P}^{[N_e \cdot N_k \times N_e]}$ is a diagonal matrix containing p_e, and $\mathbf{q}^{[N_e \cdot N_k]}$ is a vector containing q_e. As (27) is a linear inequality constraint it can be added to the optimization problem (16), given as

$$\min_{\boldsymbol{\beta},\,\mathbf{A}} \quad \mathbf{A}^\top \mathbf{L} \tag{28a}$$

$$\text{s.t.} \quad \mathbf{H}\boldsymbol{\beta} = \mathbf{R} \tag{28b}$$

$$\mathbf{C}\boldsymbol{\beta} \;-\; \mathbf{C}_m \mathbf{A} \leq \mathbf{0} \tag{28c}$$

$$-\mathbf{I}\boldsymbol{\beta} \;-\; \mathbf{P}\mathbf{A} \leq \mathbf{q} \tag{28d}$$

$$\mathbf{K}_G(\boldsymbol{\beta}_k) + \mathbf{K}(\mathbf{A}) \succeq 0 \;\forall\, k = 1, \ldots, N_k \tag{28e}$$

The local stability constraint (28d) adds $m_P = N_e \cdot N_k$ linear inequality constraint functions to the problem.

2.3.2 Final implementation

As discussed in the previous section the inclusion of the local stability constraint introduces an iterative solver process, which is shown in Algorithm 1.

Algorithm 1 Truss optimization including global and local stability

1: Initialize $\mathbf{L}$, $\mathbf{H}$, $\mathbf{R}$, $\mathbf{C}$, $\mathbf{C}_m$, $\mathbf{K}$, and $\mathbf{K}_G$
2: Solve (16) to find $\boldsymbol{\beta}_0$
3: Set $i \leftarrow 1$ and $\Delta V = 1$
4: Initialize $\mathbf{P}$ and $\mathbf{q}$ in (27) from $\boldsymbol{\beta}_0$
5: **while** $\Delta V > \varepsilon_V$ **do**
6: Solve (28) to find $\mathbf{A}_i$ and $\boldsymbol{\beta}_i$
7: Update $\mathbf{P}$ and $\mathbf{q}$ from $\boldsymbol{\beta}_i$
8: $V_i = \mathbf{A}_i^\top \mathbf{L}$ and $\Delta V = \frac{|V_{i-1} - V_i|}{V_{i-1}}$
9: $i \leftarrow i + 1$
10: **end** *while*

Line 1-2 initialize and solves the global stability problem (16) to generate an initial solution 0 to be used in the local stability constraint (27) initialized in line 4. In line 5-10 the linearization in (27) is adjusted until convergence of the change in total volume ΔV. The convergence criterion is chosen as a small number $\varepsilon_V = 10^{-3}$.

3 Numerical applications

The presented method to truss layout optimization with FELA, including global and local stability, is applied to three different two-dimensional structures. Firstly, a simple two-bar structure subject to both global and local stability issues is studied, and the numerical results are compared to the analytical solution. Secondly, a cantilever beam is studied when subject to a single and multiple point loads. Finally, a column structure subject to a vertical load is studied, and the effects of varying material parameters and slenderness ratios are investigated.

If nothing else is stated, the material parameters are given as $E = 210$ GPa and $f_y = 235$ MPa. In the result figures supported nodes are represented by solid circles while loads are applied at the white squares only. For the two latter structures, the meshes are described by the number of nodes in the x- and z-direction by n_x and n_z, respectively, and the connectivity is given by the parameter r. If $r = 1$ all nodes are connected with elements to their nearest nodes in all directions, if $r = 2$ all nodes are connected to both the nearest and next-nearest nodes in all directions, and so on.

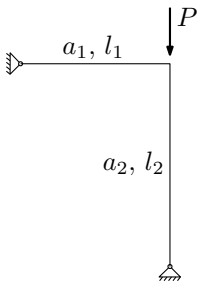

Fig. 4 Two-bar structure with load P and supports

The code was implemented in Matlab R2016b Mathworks (2016), and the convex solver was Mosek version 8.1.0.62 MOSEK (2018b). Mainly results were computed on a desktop with an Intel Core i7-6500U CPU 2.59 GHz and 32 GB RAM. The single case with beyond 8,000 elements was computed on a setup with 2x Intel Xeon Processor 2650v4 (12 core, 2.20 GHz) and 256 GB RAM.

3.1 Two-bar structure

To validate the implemented methods a simple two-bar structure is analysed initially. The structure is seen in Fig. 4 and the parameters given as $l_1 = 8$ m, $l_2 = 10$ m, and $P = 1$ MN.

The solution to the optimization problem only containing global stability (16) is given as $a_1 = 0.038$ cm^2 and $a_2 = 42.553$ cm^2. Including local stability the solution from Algorithm 1 is given as $a_1 = 0.038$ cm^2 and $a_2 = 49.247$ cm^2, hence a slight increase of a_2 to prevent column buckling.

The analytical solution to the two-bar structure including global stability is derived in Poulsen and Olesen (2015) and given as

$$a_1 = \frac{Pl_1}{El_2}, \quad a_2 = \frac{P}{f_y} \tag{29}$$

When local stability is governing the solution becomes

$$a_1 = \frac{Pl_1}{El_2}, \quad a_2 = \sqrt{\frac{P}{\alpha_2}} \tag{30}$$

hence the area of element 2 is now given by the critical Euler load (21). The analytical solution is found to $a_1 = 0.038$ cm^2 and $a_2 = 42.553$ cm^2 for global stability, and $a_2 = 49.247$ cm^2 for local stability, where α_e is given by α_{tube} and (20). The numerical solution thus corresponds to the analytical solution. Furthermore, it is noted that the cross section area of member a_1, ensuring global stability, is only about one thousandth of the cross section area of member a_2, constituting the

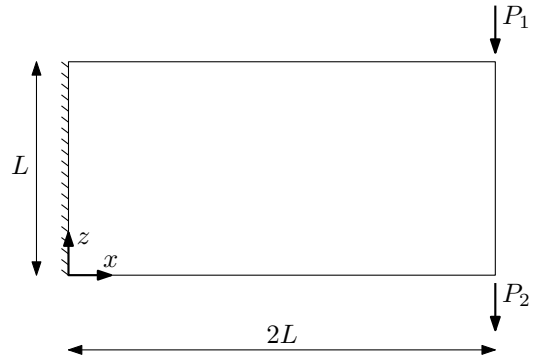

Fig. 5 Domain, boundary conditions, and loads of cantilever beam

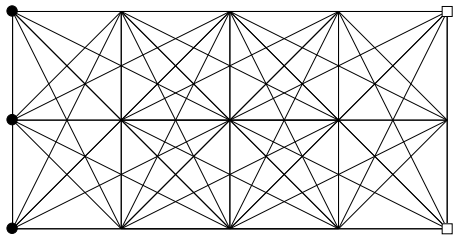

Fig. 6 Cantilever beam Case 1 and 4, initial ground structure, $N_e = 78$

main load-bearing structure. The additional volume of material to constrain the structure from global stability issues is thus almost neglectable, but crucial to the structural layout and integrity.

3.2 Cantilever beam

The well-known cantilever beam with tip loads is studied. The domain is rectangular with a side length ratio of 2:1, supported along the left edge and loaded with point loads at the upper and lower right corners. The domain, boundary conditions, and loads are seen in Fig. 5. The parameters are given as $L = 5$ m and $P_1 = P_2 = 100$ kN.

Four different cases are studied. In Case 1-3, only load P_1 is applied, whereas in Case 4 load P_1 and P_2 are applied as individual load cases. In Case 1-3, the effect of an increasing mesh density is studied. The coarser mesh used in Case 1 and 4 is seen in Fig. 6.

The mesh parameters n_x, n_z, and r are shown in Tab. 1 for the four cases, together with the number of nodes N, degrees of freedom N_d, number of elements N_e, and number of load cases N_k. Additionally, the objective values V are shown for the three types of optimization problems ((7), (16), (28)). Finally, the number of elements in the final optimized structures, above a given threshold of $10^{-2} \cdot \max(\mathbf{A})$, are shown for the three optimization problems. The threshold is chosen to remove elements with near zero-area, and given relative to the largest element area.

In Fig. 7 the optimized structures of the cantilever beam Case 1 are seen. In Fig. 7a the solution without any stability constraints is seen, hence a pure material optimization. In Fig. 7b the global stability constraint is added, and in Fig. 7c the local stability constraint is added.

From Tab. 1 and Fig. 7 it is seen how the volume is unaffected when adding the global stability constraint compared to the structure without stability constraints. That being the case, for Case 1 with coarse mesh, the final structures from the two optimization problems are almost identical, with only one additional bar in the latter. The structural layout is thus almost unchanged when including global stability in this particular case, which later is seen commonly not to be the case. When adding the local stability constraint, see Fig. 7c, the change is significant in both structural layout, number of elements, and volume. The number of elements is reduced substantially as the material is better utilized in fewer but larger elements when constraining local stability. As a result, the design is very different from the previous, and the volume is increased.

From Case 2 and 3 in Tab. 1 it is seen that when increasing the mesh density, the usual behavior of decreasing and converging volume is seen in all three optimization problems. Furthermore, it is seen that the number of elements in the structures increases with increasing mesh density. Similar to Case 1 and what was seen in Sec. 3.1, the change in volume from the structures without stability constraints to structures including global stability is insignificant.

In Fig. 8 and 9 the final result (including global and local stability constraints) for Case 2 and 3, with medium and dense meshes, are shown. In Fig. 9 only the main structure is shown with colored elements, whereas the remaining members are shown in greyscale to simplify the plot. In Fig. 8 the structure is to certain extent similar to the one in Fig. 7c with few elements and a clear structural system, though with a smoother curve on the lower compression part. On the contrary, the structure in Fig. 9 contains a large number of elements. The main structure (shown in color) is though to some degree similar to Case 1 and 2. The compression part is reduced to a few large members, whereas the tension part is distributed over many elements in a fan-like structure. This fan-like structure resembles a thin plate element, which is known to be more optimal than truss-like structures in tension Sigmund et al. (2016). Furthermore, the entire main structure is supported by several very thin members (shown in greyscale) to ensure global stability. Finally, it is noted how the relative

Table 1 Cantilever beam mesh parameters, number of load cases N_k, objective values V, and number of elements N_e above given threshold of $10^{-2} \cdot \max(\mathbf{A})$ for the three types of optimization problems

Case	Load	n_x	n_z	r	N	N_d	N_e	N_k	Objective value V [10^{-4}m^3] / $N_e > 10^{-2} \cdot \max(\mathbf{A})$		
									Without stability	With global stability	W. global and local stability
1	P_1	5	3	2	15	24	78	1	170.2 / 41	170.2 / 42	203.0 / 16
2	P_1	9	5	4	45	80	740	1	158.5 / 54	158.5 / 55	189.3 / 34
3	P_1	17	9	8	153	288	8,712	1	156.7 / 179	156.6 / 374	160.3 / 195
4	P_1 & P_2	5	3	2	15	24	78	2	180.6 / 49	180.8 / 49	207.9 / 16

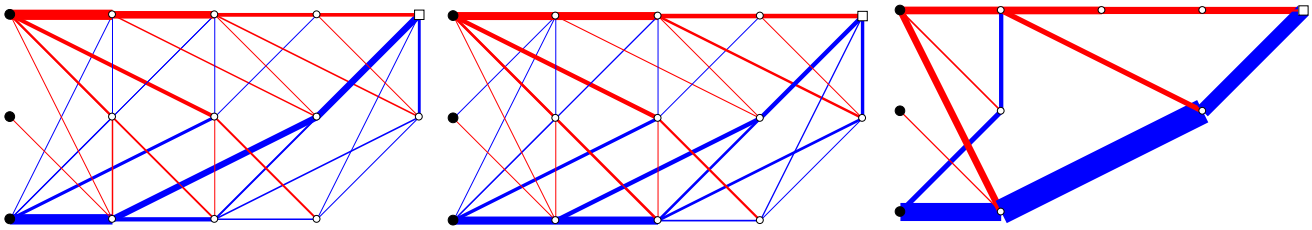

(a) Without stability, $V = 170.2 \times 10^{-4}$m^3, $N_e = 41$ (b) With global stability, $V = 170.2 \times 10^{-4}$m^3, $N_e = 42$ (c) With global and local stability, $V = 203.0 \times 10^{-4}$m^3, $N_e = 16$

Fig. 7 Solutions of cantilever beam Case 1 (coarse mesh). Color indication: blue=compression, red=tension

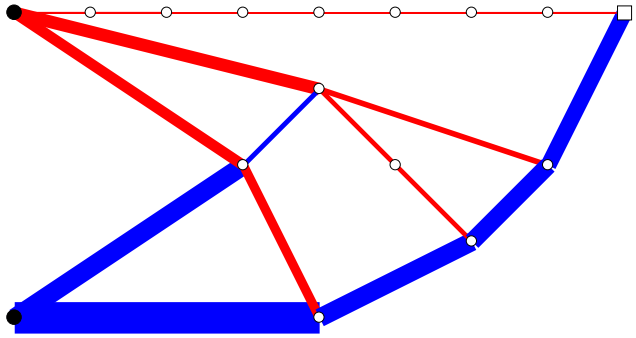

Fig. 8 Solution of cantilever beam Case 2 (medium mesh) with global and local stability, $V = 189.3 \times 10^{-4}$m^3, $N_e = 34$. Color indication: blue=compression, red=tension

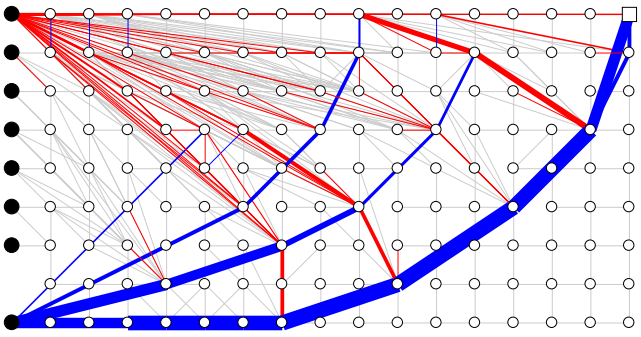

Fig. 9 Solution of cantilever beam Case 3 (dense mesh) with global and local stability, $V = 160.3 \times 10^{-4}$m^3, $N_e = 422$ (195 coloured). Color indication: blue=compression, red=tension

increase in volume when adding local stability is significantly smaller for Case 3 compared to Case 1 and 2. However, it is important to recall that when including local stability, the problem becomes concave, hence no global optima is guaranteed for direct comparison.

As a final remark to the above study, it is noted that the results of all three cases resemble the usually optimized structures of the tip loaded cantilever beam, see e.g. Changizi and Jalalpour (2017). A quantitative comparison has not been possible, as essential material parameters have not been stated in the paper.

The last study of the cantilever beam, Case 4 with two individual load cases P_1 and P_2, is seen in Fig. 10. In Fig. 10a the structure resembles the one in Fig. 7a, only subject to load P_1, but symmetric around the horizontal center axis being able also to support load P_2. Hence, including global stability in Fig. 10b does not change the structure for this particular case. Including local stability in Fig. 10c makes a significant change to the layout, where the symmetry in Fig. 10a and 10b disappears due to the asymmetry in the local stability constraint. The load P_2 is thus carried in a tension rod to the top node, utilizing the same 'expensive' compression members to carry both load P_1 and P_2.

3.3 Column structure

Here, a vertically loaded column is studied. The column is confined to a rectangular domain with fixed height H and varying width W, hence varying slenderness ratios. The column is supported along the bottom edge and loaded with a point load centered at the top. The domain, boundary conditions, and load are seen in Fig. 11.

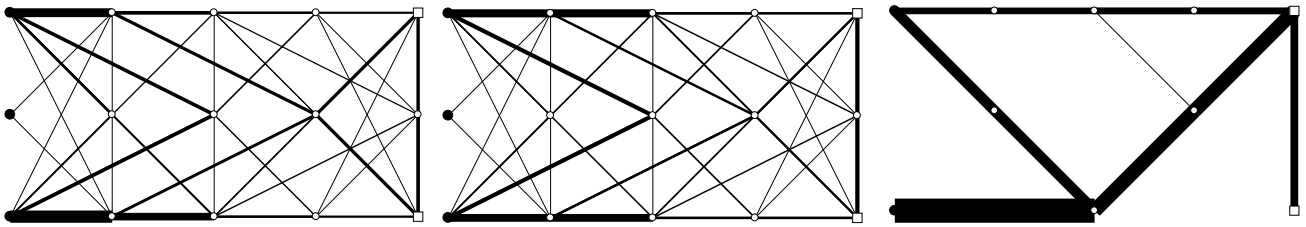

(a) Without stability, $V = 180.6 \times 10^{-4}\text{m}^3$, $N_e = 49$ (b) With global stability, $V = 180.8 \times 10^{-4}\text{m}^3$, $N_e = 49$ (c) With global and local stability, $V = 207.9 \times 10^{-4}\text{m}^3$, $N_e = 16$

Fig. 10 Solution of cantilever beam Case 4 (two load cases)

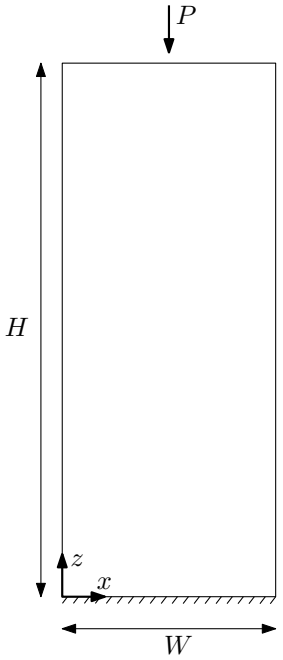

Fig. 11 Domain, boundary conditions, and loads of column structure

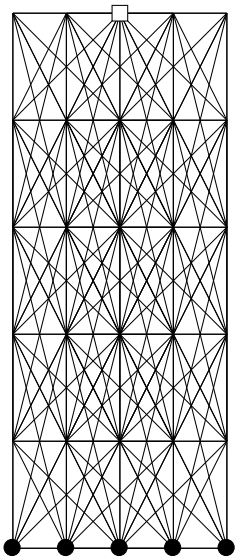

Fig. 12 Column structure Case 1 and 2, initial ground structure, $N_e = 213$

The fixed parameters are given as $H = 4$ m, $P = 10$ kN, and node connectivity $r = 2$.

Four different cases are studied. In the first case the material parameters are unity, hence $E = 1$ GPa and $f_y = 1$ MPa, and the 235 MPa in (20) is replaced with 1 MPa. For Case 2-4 the material parameters are $E = 210$ GPa and $f_y = 235$ MPa. In Case 2-4, the effect of increasing column slenderness is studied. The mesh used in Case 1 and 2 is seen in Fig. 12. It must be stated, that overlapping elements, e.g. two elements in the same plane extending from the same node to the closest and second closest node, respectively, are plotted in the same plane. In few cases, this is not the best visualization, but in general, this has been considered the most accurate way to visualize the results consistently.

The column width W and mesh parameters are seen in Tab. 2 for the four cases. Furthermore, the material parameters E and f_y are shown, as well as the objective values V and the number of elements N_e in the final structures for the three types of optimization problems.

In the first case, the material parameters are given as unity, hence the usual ratio of around 1:1000 between E (GPa) and f_y (MPa) is neglected. This particular case is included, as it is common practice to use unity material parameters in optimization benchmark examples Sigmund and Bendsøe (2003). This ratio has no effect on the results when optimizing without global stability constraints. However, when including global stability constraints in the optimization problem, this ratio has a considerable impact on the final optimized structures. Despite this, previous works such as Guo et al. (2005); Descamps and Filomeno Coelho (2014); Tugilimana et al. (2018) use unity material parameters in optimization problems with global stability constraint. Case 1 thus demonstrates the importance of using correct material parameters, when working with global stability, opposite to pure material optimization.

In Fig. 13 the results of Case 1 are seen. For comparison, the results of Case 2 (similar to Case 1, but with $E = 210$ GPa and $f_y = 235$ MPa) are seen in Fig. 14. In Fig. 13a and 14a, solutions without stability constraints, the structures are seen to be similar, as the load is carried directly from load point to boundary condition. When including the global stability constraint, Fig. 13b and 14b, the differences between the two cases are clear. In Case 1, the point load is mainly carried in the outer members with a web of thinner members in the interior. Contrary, in Case 2, the load is mainly carried by the center column, which is supported by an outer web of very thin members. When including local stability, Fig. 13c and 14c, the differences in the structural system are similar, though more pronounced. A quantitative comparison is not possible due to the different material parameters, but the qualitative comparison above shows the importance of using

Table 2 Column structure mesh parameters, material parameters, objective values V, and number of elements N_e above given threshold of $8 \times 10^{-5} \cdot \max(\mathbf{A})$ for the three types of optimization problems

Case	W [m]	n_x	n_z	N	N_d	N_e	E [GPa]	f_y [MPa]	Objective value V [10^{-6}m^3] / $N_e > 10^{-4} \cdot \max(\mathbf{A})$		
									Without stability	With global stability	W. global and local stability
1	$H/2.5$	5	6	30	50	213	1	1	40.0×10^3 / 9	643.2×10^3 / 71	710.6×10^3 / 50
2	$H/2.5$	5	6	30	50	213	210	235	170.2 / 9	170.8 / 73	290.0 / 41
3	$H/10$	3	11	33	60	204	210	235	170.2 / 19	171.3 / 77	191.2 / 66
4	$H/20$	3	21	63	120	414	210	235	170.2 / 39	172.2 / 187	178.5 / 123

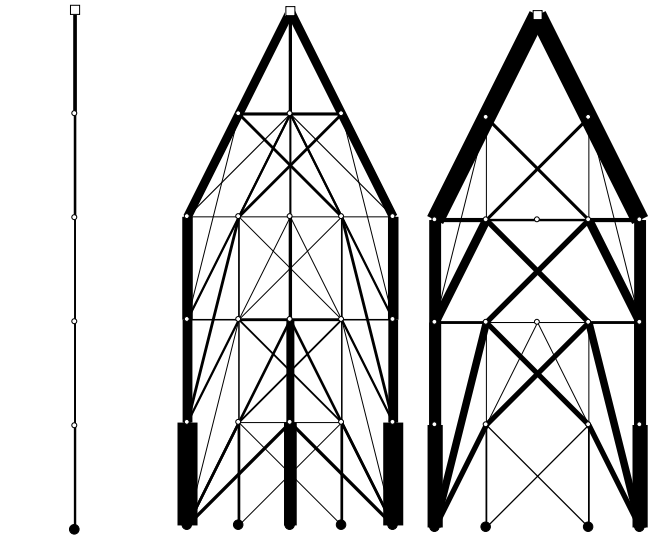

(a) Without stability, $V = 40.0 \times 10^{-3}$m^3, $N_e = 9$

(b) With global stability, $V = 643.2 \times 10^{-3}$m^3, $N_e = 71$

(c) With global and local stability, $V = 710.6 \times 10^{-3}$m^3, $N_e = 50$

Fig. 13 Solution of column structure Case 1 with unit material parameters, width $W = 4/2.5$ m

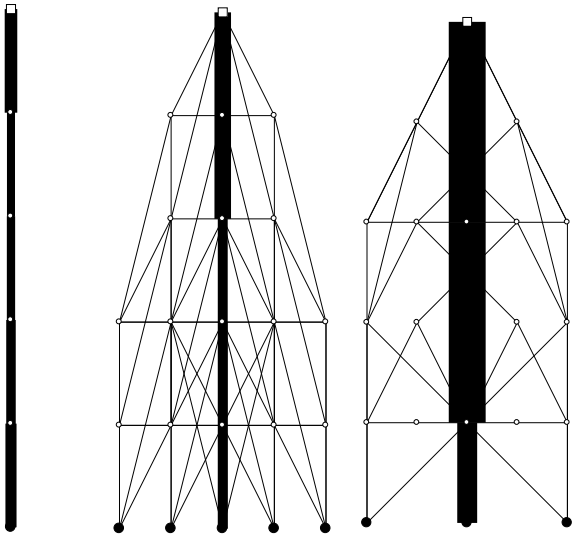

(a) Without stability, $V = 170.2 \times 10^{-6}$m^3, $N_e = 9$

(b) With global stability, $V = 170.8 \times 10^{-6}$m^3, $N_e = 73$

(c) With global and local stability, $V = 290.0 \times 10^{-6}$m^3, $N_e = 41$

Fig. 14 Solution of column structure Case 2, width $W = 4/2.5$ m

correct material parameters when working with global stability. As a final comment, it is noted that the structures from Case 1 resemble the results in Changizi and Jalalpour (2017), where a similar column structure is optimized. Again, a quantitative comparison has not been possible.

In Case 2-4, the effect on increasing slenderness is studied. The results for the three cases with increasing slenderness are seen in Fig. 14, 15, and 16. In some plots, additional elements, to the number of elements with cross section areas above the threshold shown in Tab. 2, are plotted in grey-scale. The grey-scale members are plotted to visualize kinematic stable structures, and the number of members in black is used for quantitative comparisons.

For all three cases, the structures, optimized without stability, are identical in layout and volume V, see Fig. 14a, 15a, and 16a. However, when including global stability, the differences become noticeable. In Fig. 14b the load is, as mentioned previously, mainly carried by the center column, which is supported by an outer web of very thin members to constrain global stability. In Fig. 15b the load is still mainly carried by the center column, but towards the bottom, more load is carried by the increasing outer members. In Case 4, Fig. 16b, the load is only carried by the center column in the upper part but gradually transferred to the outer members. Thus, in the lower part, the load is mainly carried by the outer members. In both Case 3 and 4, the load carrying members are supported by thin members to constraint global stability. A reason for the more slender columns to transfer the load from the center to the outer is the increased need for bending stiffness near the bottom to resist global stability problems. Another reason for this effect is the decreased distance from the load to the outer members, when slenderness is increasing.

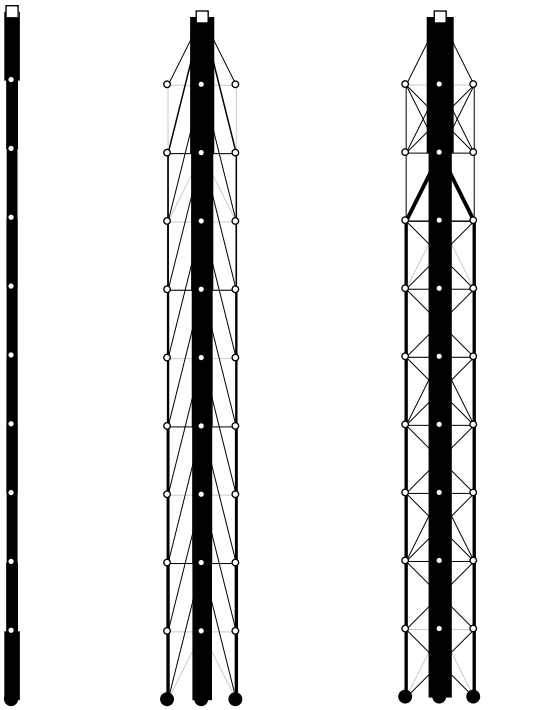

(a) Without stability, $V = 170.2 \times 10^{-6}\text{m}^3$, $N_e = 19$

(b) With global stability, $V = 171.3 \times 10^{-6}\text{m}^3$, $N_e = 95$ (77 in black)

(c) With global and local stability, $V = 191.2 \times 10^{-6}\text{m}^3$, $N_e = 75$ (66 in black)

Fig. 15 Solution of column structure Case 3, width $W = 4/10$ m

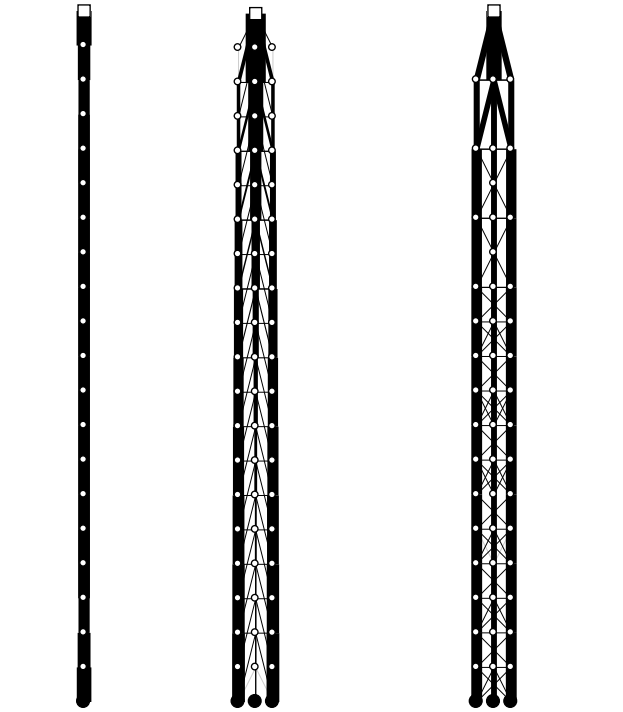

(a) Without stability, $V = 170.2 \times 10^{-6}\text{m}^3$, $N_e = 39$

(b) With global stability, $V = 172.2 \times 10^{-6}\text{m}^3$, $N_e = 192$ (187 in black)

(c) With global and local stability, $V = 178.5 \times 10^{-6}\text{m}^3$, $N_e = 125$ (123 in black)

Fig. 16 Solution of column structure Case 4, width $W = 4/20$ m

The 'cost' in material used to transfer the load to the outer members is thus reduced by increasing slenderness. As an additional note, it is remarked that for the more slender columns, the increase in volume, from the structures without stability to the once with global stability, is more significant. However, it is noted that the increase, in general, is small, similar to what was seen in both Sec. 3.1 and 3.2. It is thus a general trend, that including global stability does not increase the volume significantly, but has a large impact on the structural layout.

When including the local stability constraint, for all three cases the effects discussed above are more pronounced, see Fig. 14c, 15c, and 16c. Similar to the cantilever structures discussed in Sec. 3.2, the increase in volume when including local stability is likewise significant for all three column cases. The relative increase is though reduced for the more slender columns, where the material utilization is better.

4 Conclusions

In this paper, a new method to handle global and local stability simultaneously in truss optimization was presented. The method was based on the finite element limit analysis method, allowing very efficient state-of-the-art convex solvers to be used in solving the established optimization problem. The global stability constraint was solved by the introduction of a semidefinite constraint, whereas local stability was handled through the critical Euler buckling load. The overall concave problem was solved in an iterative process with convex sub-problems.

The proposed method was demonstrated through three different applications. The implementation of the method was validated against the analytical solution of a simple two-bar structure. The study of the cantilever beam with tip loads proved the convergence properties of the method by increasing mesh densities. The convergence in decreasing material volume was seen for all three optimization problems; pure material optimization, including global stability, and including both global and local stability. With the vertically loaded col-

umn structure, the importance of using correct material parameters, when including global stability in the optimization problem, was treated. Hence, the usual practice of using unity material parameters in optimization benchmark examples was challenged by comparison of the structural layout of two identical optimization problems, only differing in applying unity and real material parameters, respectively. The result clearly showed the difference and underlined the recommendation of using correct material parameters in structural optimization including stability. Furthermore, all three studies indicated how the effect of including global stability was small on the volume but made a significant impact on the structural layout. Including local stability led in general to a significant volume increase, and did in several cases also lead to considerable changes in the structural design.

In general, the studies and findings emphasized the eligibility and potential of the method. The main contribution of this paper is thus a newly proposed approach to efficient truss optimization including global and local stability. Hence, the presented basic formulations of the FELA based optimization problem including global stability, and the proposed algorithm handling the linearized local buckling constraint, form a basis for further studies and method development.

The perspectives of further development are promising, but with several challenges to cope. The large-scale perspectives in the present formulations and in combination with the Mosek solver are limited. Hence, to utilize the method fully in practical applications, where a large amount of elements are desirable to accommodate larger design freedom, some challenges are to be overcome. Another challenge is the local stability constraint leading to a concave optimization problem, hence only local minima as solutions. Possible methods to search the solution space towards more optimal solutions are thus desirable. Finally, methods to reduce the truss complexity, hence number of elements in the final optimized designs, especially desirable for trusses with dense initial meshes, are of interest towards practical applications.

Replication of Results The presented work is part of an industrial ph.d. project. Due to property rights from the commercial partner, COWI A/S, it has not been possible to make the code available as supplementary material.

Funding This study was funded by the COWI Foundation grant C-131.02 and Innovation Fund Denmark grant 5189-00112B.

Conflict of Interest The authors declare that they have no conflict of interest.

References

Achtziger W (1999a) Local stability of trusses in the context of topology optimization. Part I: Exact modelling. Structural Optimization 17(4):235–246, DOI 10.1007/s001580050056

Achtziger W (1999b) Local stability of trusses in the context of topology optimization Part II: A numerical approach. Structural Optimization 17(4):247–258, DOI 10.1007/s001580050056

Akhlaghi T (2006) Finite element lower bound limit analysis in soil mechanics using non-linear programming. Wseas Transactions on Advances in Engineering Education 3(8)

Anderheggen E, Knöpfel H (1972) Finite element limit analysis using linear programming. International Journal of Solids and Structures 8(12):1413–1431, DOI 10.1016/0020-7683(72)90088-1

Ben-Tal A, Jarre F, Kočvara M, Nemirovski A, Zowe J (2000) Optimal Design of Trusses Under a Nonconvex Global Buckling Constraint. Optimization and Engineering 1:189–213, DOI 10.1023/A:1010091831812

Changizi N, Jalalpour M (2017) Topology optimization of steel frame structures with constraints on overall and individual member instabilities. Finite Elements in Analysis and Design 141(March 2017):119–134, DOI 10.1016/j.finel.2017.11.003

Cook RD, Malkus D, Plesha M (1989) Concepts and Applications of Finite Element Analysis. DOI 10.1115/1.3264300

Damkilde L, Høyer O (1993) An efficient calculations implementation of limit state based on lower-bound solutions. Computers & Structures 49(6):953–962

Descamps B, Filomeno Coelho R (2014) The nominal force method for truss geometry and topology optimization incorporating stability considerations. International Journal of Solids and Structures 51(13):2390–2399, DOI 10.1016/j.ijsolstr.2014.03.003

Dorn WS, Gomory RE, Greenberg HJ (1964) Automatic design of optimal structures. Journal de Mecanique 3(1):25–52

Evgrafov A (2004) On globally stable singular topologies. Structural and Multidisciplinary Optimization 29(2148):1–13, DOI 10.1007/s00158-004-0428-6

Fin J, Alves L, Eduardo B, Fancello A (2018) Structural topology optimization under limit analysis. Structural and Multidisciplinary Optimization

Guo X, Cheng GD, Olhoff N (2005) Optimum design of truss topology under buckling constraints. Structural and Multidisciplinary Optimization 30(3):169–180, DOI 10.1007/s00158-004-0511-z

He L, Gilbert M (2015) Rationalization of trusses generated via layout optimization. Structural and Multidisciplinary Optimization 52(4):677–694, DOI 10.1007/s00158-015-1260-x

Herfelt MA (2017) Numerical Limit Analysis of Precast Concrete Structures. Phd thesis, Dept. of Civil Engineering, Technical University of Denmark

Herfelt MA, Poulsen PN, Hoang LC, Jensen JF (2016) Numerical limit analysis of keyed shear joints in concrete structures. Structural Concrete 17(3):481–490, DOI 10.1002/suco.201500161

Herfelt MA, Poulsen PN, Hoang LC, Jensen JF (2017) Lower bound plane stress element for modelling 3D structures.

Proceedings of the Institution of Civil Engineers - Engineering and Computational Mechanics pp 1–11, DOI 10.1680/jencm.16.00026

Herfelt MA, Poulsen PN, Hoang LC, Jensen JF (2018) Lower bound multiscale element for in situ cast joints in triaxial stress. Engineering Structures 167(November 2017):340–350, DOI 10.1016/j.engstruct.2017.12.054

Herfelt MA, Poulsen PN, Hoang LC (2019) Strength-based topology optimisation of plastic isotropic von Mises materials. Structural and Multidisciplinary Optimization 59(3):893–906, DOI 10.1007/s00158-018-2108-y

Kočvara M (2002) On the modelling and solving of the truss design problem with global stability constraints. Structural and Multidisciplinary Optimization 23(3):189–203, DOI 10.1007/s00158-002-0177-3

Krabbenhoft K, Damkilde L, Krabbenhoft S (2005) Ultimate limit state design of sheet pile walls by finite elements and nonlinear programming. Computers & Structures 83(4-5):383–393, DOI 10.1016/j.compstruc.2004.08.016

Krabbenhøft K, Lyamin AV, Sloan SW (2008) Three-dimensional Mohr-Coulomb limit analysis using semidefinite programming. Communications in Numerical Methods in Engineering 24:1107–1119, DOI 10.1002/cnm

Krenk S (1994) Limit analysis and optimal design of plates with equilibrium elements. Journal of Engineering Mechanics 120(6)

Lyamin AV (2009) Limit analysis of bearing capacity of eccentrically loaded strip footing on clay with tension cut-off interface conditions. Computational Geomechanics, Comgeo I - Proceedings of the 1st International Symposium on Computational Geomechanics

Madah H, Amir O (2017) Truss optimization with buckling considerations using geometrically nonlinear beam modeling. Computers and Structures 192:233–247, DOI 10.1016/j.compstruc.2017.07.023

Mathworks (2016) MATLAB R2016b

Mikkelsen LSM (2018) Strength based optimization of truss structures including stability. M.Sc. thesis, Technical University of Denmark, Kgs. Lyngby, Denmark

MOSEK (2018a) Mosek Modeling Cookbook 3.1. Tech. Rep. May

MOSEK (2018b) The MOSEK optimization toolbox for MATLAB manual. Version 8.1.

Parkes EW (1975) Joints in optimum frameworks. International Journal of Solids and Structures 11(9):1017–1022, DOI 10.1016/0020-7683(75)90044-X

Pedersen P (1972) On the optimal layout of multi-purpose trusses. Computers and Structures 2(5-6):695–712, DOI 10.1016/0045-7949(72)90032-6

Poulsen PN, Damkilde L (2000) Limit state analysis of reinforced concrete plates subjected to in-plane forces. International Journal of Solids and Structures 37(42):6011–6029, DOI 10.1016/S0020-7683(99)00254-1

Poulsen PN, Olesen JF (2015) Bærende konstruktioner 1. Polyteknisk Forlag

Rozvany G (1996) Difficulties in truss topology optimization with stress, local buckling and system stability constraints. Structural Optimization 11(3-4):213–217, DOI 10.1007/BF01197036

Sigmund O, Bendsøe MP (2003) Topology Optimization - Theory, Methods and Applications. DOI 10.1007/978-3-662-05086-6

Sigmund O, Aage N, Andreassen E (2016) On the (non-)optimality of Michell structures. Structural and Multidisciplinary Optimization 54(2):361–373, DOI 10.1007/s00158-016-1420-7

Torii AJ, Lopez RH, Miguel LF (2015) Modeling of global and local stability in optimization of truss-like structures using frame elements. Structural and Multidisciplinary Optimization 51(6):1187–1198, DOI 10.1007/s00158-014-1203-y

Tugilimana A, Filomeno Coelho R, Thrall AP (2018) Including global stability in truss layout optimization for the conceptual design of large-scale applications. Structural and Multidisciplinary Optimization 57(3):1213–1232, DOI 10.1007/s00158-017-1805-2

Weldeyesus AG, Gondzio J, He L, Gilbert M, Shephard P, Tyas A (2019) Adaptive solution of truss layout optimization problems with global stability constraints. Structural and Multidisciplinary Optimization DOI 10.1007/s00158-019-02312-9

Zhou M (1996) Difficulties in truss topology optimization with stress, local buckling and system stability constraints. Structural Optimization 11(3-4):213–217, DOI 10.1007/BF01197036